Small-Angle X-ray Scattering Study of Craze Formation and Dynamics in Thermoplastics

G. J. Salomons, M. A. Singh,* T. Bardouille, and W. A. Foran

Queen's University, Department of Physics, Kingston, Ontario, Canada K7L-3N6

M. S. Capel

Brookhaven National Laboratory, Upton, New York 11973

Received May 4, 1998; Revised Manuscript Received November 18, 1998

ABSTRACT: A detailed investigation of the microscopic mechanisms of tensile stress deformation was performed. The experiments involved two different thermoplastic materials: high impact polystyrene (HIPS) and a novel polystyrene (PS)−polybutadiene (PB) blend, at temperatures ranging from 30 to 70 °C, deformed at a constant uniaxial strain rate. Real-time measurements of the applied stress, X-ray absorption by the sample, and small-angle scattering were used to identify the presence of shear and craze deformation stages. Craze fibril surface energies were determined from calculations of the fibril diameter in order to distinguish between craze growth by the competing mechanisms of chain scission and forced reptation.

1. Introduction

The use of additives to enhance the toughness of thermoplastic materials is fundamental to the process of developing new polymers for a large class of applications. An understanding of the role played by these additives at a microscopic level is required in order to achieve maximum effectiveness. The commonly observed process of crazing is one of the most complex modes of polymer deformation, being linked with enhanced toughening, while at the same time developing into pure cracks, making them a precursor to failure. For this reason, studies of the fundamental mechanisms controlling craze formation and growth continue to be prominent in polymer deformation research.

The formation and growth of crazes depend upon both the large scale structure of the polymer material and interactions between individual polymer molecules within craze fibrils. Craze growth is controlled by the response of load-bearing fibril molecules, which support the applied stress to a significant degree.[1] The craze fibril surface energy is a measure of the motion of individual molecules; correlations between this surface energy and the macroscopic parameters of temperature, molecular weight, and applied force, therefore, provide a means of probing molecular dynamics in polymers.

As craze fibril molecules are drawn out of the bulk polymer, the energy required to form a new fibril surface is dependent upon the forces driving the competing processes of chain scission and reptation. The scission force is due to the energy required to break a polymer chain and is a function of the molecular weight and density. The reptation force is due to the energy required for polymer chains to move past each other and varies with moelcular weight, strain rate and temperature. The rate of craze growth, and hence its effect on material toughness, will be determined by the dominant force.

The fibril surface energy in thin films of pure polystyrene (PS) has been measured as a function of temperature[2] to identify the transition from craze growth by scission to that of craze growth by reptation. From these measurements it was verified that forced reptation processes prevail in the crazing mechanism. It is of interest to perform a similar study of bulk composite materials to confirm that the molecular-level processes observed in the pure PS thin films persist for three-dimensional materials containing toughening additives.

It has long been known[3] that PS can be toughened by incorporating 10−20 wt % of a low-molecular weight additive such as polybutadiene. This is the basis of the material known as high impact polystyrene (HIPS). The enhanced toughening has traditionally been attributed to craze promotion, wherein the existing rubber particles act as craze nucleation sites by locally reducing the energy required to nucleate crazes.[4] It has been suggested that the PB in HIPS may perform an additional function: cavitation of the PB domains, producing voids, which may act as localized centers of strain relief or merge to form crazes.[5]

Yet another mechanism of toughening thermoplastics has been suggested in which small amounts (up to 4%) of low molecular weight PB are added to PS.[6] Pools of liquid rubber, too small to initiate crazes, are formed in the PS matrix. The liquid is thought to be absorbed into the active region surrounding a craze where it serves to plasticize the polymer molecules, thereby enhancing their mobility. This greatly increases the craze velocity and subsequently the strain energy which can be absorbed by a craze.[7] The plasticization mechanism is quite distinct from what is believed to occur in HIPS, and the craze structure observed in these two materials can be expected to reflect this difference.

Real-time studies of material deformation are essential to any attempt to identify the relation of crazing to the alternative deformation mechanisms of shear banding[8,9] and rubber-particle cavitation.[5,10] Small-angle X-ray scattering (SAXS) is an ideal, noninvasive tool for examining craze structure in bulk materials.[9,11−15] Accurate implementation of real-time experiments requires a method of generating consistent craze deformation in conjunction with in-situ, real-time small-angle

10.1021/ma980709e CCC: $18.00
Published on Web 02/04/1999

Table 1. Glass Transition Temperatures for the Sample Materials

material	T_g (±0.5), °C
PS	106.7
PS + 1 wt % PB blend	103.2
PS + 2 wt % PB blend	102.1
PS + 5 wt % PB blend	101.0
HIPS	97.6

X-ray scattering (RTSAXS) measurements. An apparatus has been developed for this purpose[16] which allows the application of tensile deformation with varying strain rates and sample temperatures, while holding the sample center motionless relative to the X-ray beam. This typically requires a synchroton source where the available high flux makes it possible to obtain very high quality data on relatively short time scales.

The role of crazing in the overall deformation process and the mechanisms governing craze formation and growth were investigated through a series of constant strain rate tensile deformation experiments, performed on samples of two representative thermoplastic materials, at temperatures ranging from 30 to 70 °C. Data obtained from these experiments include measurements of the stress applied to the deforming sample, X-ray absorption by the sample, and two-dimensional SAXS diffraction patterns from the sample as a function of time. This information is used to identify stages at which the deformation proceeds via crazing. Details of the craze fibril structure are examined in light of the proposed different mechanisms of craze formation and changes to the surface energy with sample temperature are compared with the predictions of the theory of craze growth by forced reptation.

2. Experimental Section

2.1. Materials. Two materials were studied in the deformation experiments: high impact polystyrene (HIPS) and, following the report of Brown et al.,[6] a custom blend of polystyrene (PS) and low molecular weight polybutadiene (PB). The HIPS material (DOW Canada Styron 484C) was obtained in the form of compression molded 2 mm thick sheets. The second material was prepared by the Industrial Materials Institute (IMI) using DOW Canada Styron 685D PS, with a molecular weight of about 300 000 and a polydispersity of about 2.4, and RICON RESINS, Inc., PB of a molecular weight of about 2000. These components were blended to an 8.5 wt % concentrate with the PS by passing it twice through a co-rotating twin-screw extruder running at 400 rpm at a temperature of 175−180 °C. From this concentrate, blends of 5, 2, and 1 wt % were produced by the addition of neat PS via an extensional flow mixer. These materials were then molded by DOW Canada following a procedure identical to that used to prepare the HIPS material. The glass transition temperatures (T_g) of the materials were measured using differential scanning calorimetry (DSC) at the Department of Chemistry, Queen's University. The DSC results are shown in Table 1. Preliminary examinations resulted in the selection of the 2 wt % blend for further experiments as this material exhibited the highest degree of toughness.

The samples were cut into 30 mm by 12 mm pieces using a water-cooled diamond saw to minimize the size and number of defects produced by the cutting process. Slotted indentations of 3 mm width were cut to a depth of 4.0 mm, with a resulting minimum height of 4.0 mm at the middle of the sample (see Figure 1). This provides a well-defined region for stress concentration. Holes of 2.0 mm diameter were drilled near the ends of the sample for attachment to the sample holders.

A mean cross-sectional area of 9.0 ± 0.1 mm^2 in the stress concentration region of the samples was calculated from an average active height (Figure 2). An active length of 1.5 ± 0.1 mm was obtained using a cross-sectional area weighting. These values are used to estimate the applied stress and strain response for the samples and were confirmed by post-mortem observations of stress whitening in the deformed samples. The calculations are based on assumptions that the proportion of strain at a given point in the sample is linearly related to the cross-sectional area of the sample at that point, and that no strain occurs outside of the stress concentration region. Applied stress is then calculated by dividing the measured force by the average cross-sectional area. The strain is calculated by dividing the change in sample length by the average active length. It should be noted that the active length of the samples is smaller than the X-ray beam spot size of 2 mm in diameter.

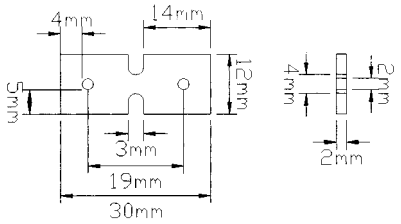

Figure 1. Illustration of the sample shape including dimensions.

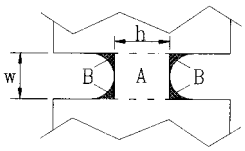

$$V_s = (A + B)t = \mathrm{h}wt + \mathrm{w}^2 t\left(1 - \frac{\pi}{4}\right)$$

$$\bar{A}_s = V_s/\mathrm{w} = \mathrm{h}t + wt\left(1 - \frac{\pi}{4}\right)$$

$$\bar{\mathrm{w}} = \mathrm{w}\int_0^{\pi/2} \sin(\theta)\cos(\theta)d\theta = \mathrm{w}/2$$

Figure 2. Calculation of the average cross-section ($\bar{A}_s$) and active strain length ($\bar{w}$).

2.2. Craze Growth Experiments. The experiments were performed at the National Synchrotron Light Source (NSLS) on the SAXS beamline, X12B.[17] The source was a circular beam approximately 2 mm in diameter with a wavelength of 1.59 Å. The detector used was a 512 × 512 pixel two-dimensional delay line proportional counter,[17] 10 cm × 10 cm in size, mounted on the end of an evacuated beampath which could be varied in length to adjust the available angular range and resolution. Two different sample-to-detector distances were used: 2.445 m and 1.000 m, with corresponding scattering angle ranges of 5.3×10^{-3} Å^{-1} < q < 7.3×10^{-2} Å^{-1}, and 0.01 Å^{-1} < q < 0.18 Å^{-1} ($q = (4\pi/\lambda)\sin\theta$).

The sample chamber used for in situ RTSAXS experiments, described by Salomons et al.,[16] includes a direct radiant heating technique to provide uniform temperatures across the sample of up to 200 °C with 0.5 °C precision. An Entran load cell, accurate to ±5 N and capable of withstanding loads of up to 4.45 × 10^2 N at temperatures up to 120 °C, is permanently incorporated into the chamber.

SAXS experiments were performed at temperatures ranging from room temperature (~30 °C) to 70 °C with a constant tensile strain rate of 5×10^{-4} s^{-1}. These rates are on the order of 10^6 times slower than the impact speeds used by Bubeck et al.[13] A timed series of 25−35 X-ray scattering measurements, time slices, were recorded using the two-dimensional wire-based detector. Each measurement consisted of an integration time of 3−10 s in duration. Prior to these measurements, a long-time (1 min) scan of undeformed sample material was performed to provide a background reference. In addition to the X-ray scattering and applied stress measurements, ratios of X-ray intensity entering and exiting the sample were recorded for each time slice.

2.3. Transmission Measurements. The ratios of transmitted intensity to the incident intensity ($\tau = I_{out}/I_{in}$) are

converted to a mass-normalized X-ray attenuation parameter, $\hat{\rho}_{ab}$, by the relation

$$\hat{\rho}_{ab} = \frac{\ln(\tau)}{\ln(\tau_o)} \tag{1}$$

where τ_o is the transmission ratio prior to the onset of deformation. Two processes can alter the measured X-ray intensity ratios: changes in sample thickness, and changes in sample density

$$\tau = \exp(-\rho z(\mu/\rho)) \tag{2}$$

Here ρ is the density, z is the sample thickness, and μ/ρ is the X-ray mass absorption coefficient which is expected to remain constant.[18] The X-ray attenuation parameter can then be used to measure changes in the sample thickness and density as a function of strain in the tensile direction (ϵ_1).

$$\hat{\rho}_{ab} = \frac{\rho(\epsilon_1)z(\epsilon_1)}{\rho(0)z(0)} \tag{3}$$

During elastic and shear deformation, where necking occurs, the sample density may be approximated as constant. This leads to a gradual decrease in $\hat{\rho}_{ab}$, in proportion to the sample thickness.

At the onset of craze or other void formation, regions of empty space are formed and the effective polymer density changes significantly. Within a craze, the volume fraction of empty space has been shown to remain constant[19] and the sample density is given by

$$\rho(\epsilon_1) = \rho(0)\left[1 - \frac{v_f V_{cr}(\epsilon_1)}{V_o}\right] \tag{4}$$

where $V_{cr}(\epsilon)$ is the craze volume at a given strain, ϵ, V_o is the total sample volume irradiated by the X-ray beam, and v_f is the volume fraction of the craze fibrils.

As growth of the crazes becomes the dominant deformation mode, the craze volume can be considered to be expanding purely by the increase in the total length of the craze fibrils.[5] This results in a linear relation between $\hat{\rho}_{ab}$ and the macroscopic strain. Observations of such linear behavior at late stages in the deformation process can be considered to be an indicator of deformation by pure craze growth.

2.4. Invariant. The invariant, a measure of the volume of scatterers present in a system, will not change in response to shear deformation, but will be strongly affected by the presence of dilatational strain due to voids. Thus, the onset of changes in the scattering invariant may be interpreted as signalling the onset of craze formation. The form of the invariant for craze fibril structures, Q_f, is given by[11]

$$Q_f = \int_0^\infty q\, dq\, I(q) = 2\pi(\rho_1 - \rho_2)^2 v_1 v_2 A L^2 \tag{5}$$

Here $I(q)$ is the scattering intensity, $(\rho_1 - \rho_2)$ is the electron density contrast, A is the cross-sectional area of the craze fibrils, L is the length of the fibrils, and v_1 and v_2 are the volume fractions of the craze voids and the polymer matrix. In the case of polymer deformation, the scattering is due to the electron density contrast between polymer matter and voids within the material.

The true invariant cannot be obtained as it requires a measure of the scattering at all angles. The effective invariant, Q_e, a measure of the contribution to the invariant from the scattering range under investigation, provides information regarding the volume of scatterers with length scales corresponding to the q range used. It may be calculated from the data by

$$Q_e \simeq \delta q \sum_{i=1}^{n} q I_f(q) \tag{6}$$

where $I_f(q)$ is the background-subtracted intensity in the craze fibril direction, δq is the pixel-to-q conversion factor, and the sum is over all valid data points. Since the invariant is often incorporated into standard SAXS models to obtain measurements of the fibril diameter and is also commonly used to estimate the strain volume attributable to crazing,[9,13] it is important to ensure that the effective invariant is a valid approximation of the true scattering invariant. This may be done by examining the relative contributions to the effective invariant from different lengthscales, as indicated by volume plots ($I \times q$ vs q). The total area under such a curve is the effective invariant.

2.5. Treatment of Two-Dimensional Scattering Patterns. Qualitative analysis of the two-dimensional scattering patterns obtained from the position-sensitive detector provides a means of distinguishing between craze and rubber-particle cavitation. Rubber-particle cavitation results in a largely isotropic scattering pattern,[20] while scattering from crazes exhibits a unique anisotropic shape.[11] Using this knowledge, direct observation of background-subtracted scattering patterns of deformed samples can be used to identify the presence of cavitation and craze formation.

Quantitative analysis of the scattering profiles was performed on one-dimensional intensity profiles of the craze fibril scattering obtained from the raw two-dimensional measurements using calibration, background subtraction, and data reduction procedures described in detail elsewhere.[21] Great care was taken in isolating craze fibril scattering from the two dimensional profiles through a comparison of the sector intensity as a function of orientation angle. The resulting one-dimensional data was used to obtain a measure of the effective invariant and the real-space distance distribution function.[22,23] Consideration of three distinct models of the scattering from craze fibril structures, compared elsewhere[21] through a rigorous series of statistical tests, leads to the result that an assumption of diffuse fibril boundaries provides the most accurate description of craze fibril scattering. This model was used to obtain reliable fibril diameter values from the scattering data which agree with the results of the real-space distribution function obtained through indirect transform methods.[23]

These intensity profiles were used to obtain measurements of the effective invariant, real-space distance distribution functions and fibril diameters.

2.6. Distance Distribution Functions. Distance distribution functions, which provide real-space information from the scattering intensity profiles, were obtained using indirect transformation based on regularization theory.[22−26] This information is complementary to that obtained by conventional Porod-based models. Distance distribution functions are best used as a guide to the general structure, as it is often quite difficult to extract meaningful information about the details of complex, inhomogeneous objects. It has been demonstrated that the transform technique works well even with a lack of low-q data,[27] and thus low-q approximations, which may affect the scattering invariant, are not required.

The program GNOM, Version E4.2, written by D.I. Svergun,[28] is used for the indirect transform analysis, with monodisperse rodlike particle form and data corrections for the anisotropy. More details of the application of this program to our present data are given elsewhere.[21] The resulting distance distribution function, $P(r)$, obtained from the GNOM program is defined by

$$P(r) = r\gamma_f(r) \tag{7}$$

where $\gamma_f(r)$ is the fibril correlation function. Maxima and minima in $P(r)$ can be used to identify fibril and void structures in the crazes and to estimate their size.

2.7. Fibril Diameters. It has been shown that the fibril diameters can be obtained using the *sigmoidal-gradient* variation on Porod's law.[21] This model describes the fibrils as having diffuse boundaries with the density following a Gaussian distribution.[29,30] The model predicts an intensity dis-

tribution at high-q given by

$$I_s(q) = \frac{K}{q^3} e^{-\sigma_s^2 q^2/2} \tag{8}$$

with I_s, q, and K being the intensity, momentum transfer, and Porod constant, respectively. The standard deviation, σ_s, is the distance from the nominal particle boundary to the point at which the density is 0.856 of that at the center of the particle.

Mean fibril diameters, $\bar{D}_s$, are calculated from the *sigmoidal-gradient* model using the relation

$$\bar{D}_s = \frac{4Q_f}{\pi(1 - v_f)K} \tag{9}$$

The invariant, Q_f, used above to calculate $\bar{D}_s$, is defined by eq 5 and approximated using eq 6. The accuracy of the effective invariant in approximating the true invariant is limited by the upper and lower q values of the data, q_{max} and q_{min}. No reliable method has been suggested to correct the invariant for the lack of low-q intensities. However, it is possible, as described by Bubeck et al.,[5] to account for the lack of high-q data by extrapolating Porod's law to infinity and adding this correction term, Q_{tail}, to eq 6. This cannot be done exactly for the *sigmoidal-gradient* model since the integral $\int_0^\infty I_s(q)\, dq$ does not converge. Therefore, the correction for the ideal Porod's law

$$Q_{tail} = \frac{K}{q_{max}} \tag{10}$$

is applied. In the ideal case, this correction results in a slight over-estimation of the fibril diameters as intensities which follow the *sigmoidal-gradient* model will fall off more rapidly, and thus have smaller Q values, than predicted by Porod's law. In reality, it is impossible to obtain an accurate estimate of the precision of the correction in the absence of a detailed knowledge of the scattering at angles larger than q_{max}.

3. Results and Discussion

3.1. Deformation Mode Identification. Plots of typical stress−strain, X-ray attenuation, and invariant curves are shown in Figure 3. At low strain levels, the stress−strain curves for both materials are approximately linear and the X-ray attenuation parameter decreases gradually in a linear fashion. The shallow decrease in the X-ray attenuation parameter suggests that no void formation is occurring; observed changes in this parameter are readily attributed to shear deformation, which causes a slight thinning of the sample.[31] The observed presence of shear deformation may be attributed to the strain rates used, which are significantly lower than those reported by other researchers.[5,7,20] Low strain rates allow for longer relaxation times and thus enable observation of slower processes, such as shear deformation.

In this HIPS material no detectable change in the invariant occurs until about 25% strain at all temperatures examined, indicating that no void formation occurs over the measured length scales during this period. Beyond this point, the invariant increases quite rapidly, accompanied by a more rapid linear decrease in the X-ray attenuation parameter. These changes signal the onset of craze formation. The onset of crazing at 25% strain is consistent with the interpretation of Bubeck et al.[5] that crazing is responsible for little more than half of the total strain-to-failure. In the PS−PB blend, a small, but steady, increase in the invariant can be observed from the onset of tensile stress. The steady increase in the invariant for the PS−PB blend material

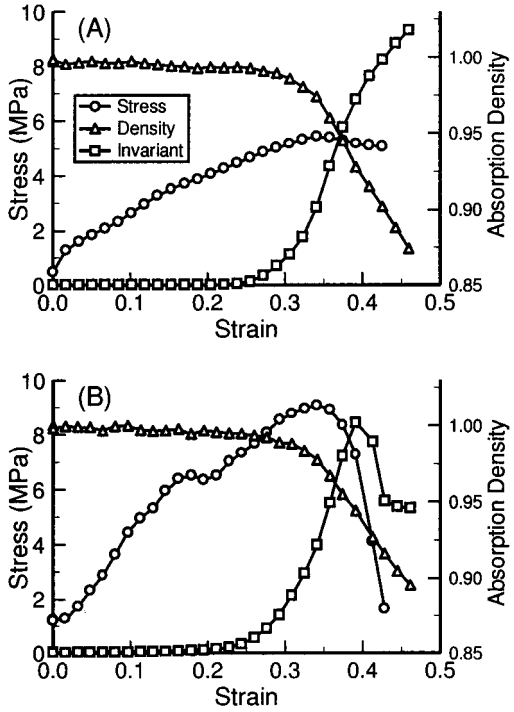

Figure 3. Applied stress (○), normalized X-ray attenuation (△), and invariant (□) curves for HIPS at 65 °C (A) and for the PS−PB blend at 67.5 °C (B).

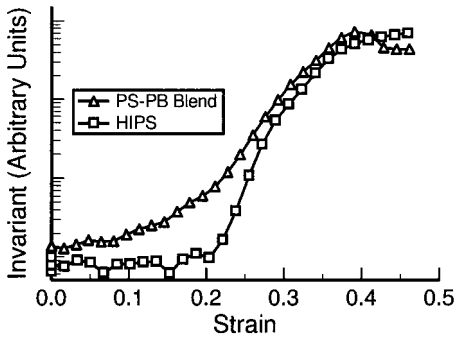

Figure 4. Invariant curves from Figure 3 plotted on a log scale. On this scale, differences between HIPS (□) and PS−PB blend (△) can be observed early on in the deformation process.

can be observed more clearly in the semilog plot of Figure 4. This change in the invariant, seen at the onset of applied stress, demonstrates that void formation occurs throughout the deformation process in this material.

The late stages of the stress−strain curves for the two materials are quite different. In the PS−PB blend a sharp decrease in stress follows the yield point, after which sample failure occurs. In the HIPS material the maximum applied stress was typically observed to be 10−20% less than in the PS−PB blend, with extended constant stress regions indicating plastic deformation. Typical maximum strains of 40−50% were found in the HIPS material and these values are consistent with the literature.[32]

The two materials are clearly seen to exhibit distinct deformation processes: while both materials undergo craze deformation, the onset of void formation occurs much earlier in the PS−PB blend while only the HIPS material undergoes extensive plastic flow. The lack of any scattering changes at low strain levels in the HIPS material is most readily attributed to expansion of the

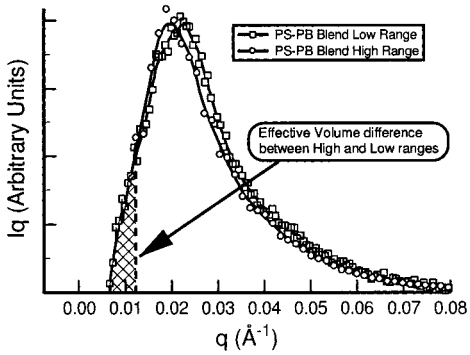

Figure 5. Volume plots for high-q (○) and low-q (□) range data, indicating the difference in the effective invariant calculated for these two ranges. (Data from PS−PB blend samples at 67.5 and 65 °C.

rubber particle additive.[10] The PS−PB blend has a yield point at higher stress values than in HIPS but has almost no extension beyond this point. Both facts point to a poorer mobility of the polymer chains in this material, indicating that the liquid rubber additive is not as effective in promoting toughness as the higher molecular weight additive in the HIPS material.

Typical volume plots for the PS−PB blend material are shown in Figure 5. From these plots it can be seen that the volume contribution from different length scales contains a well-defined peak at $q \approx 0.02$ Å^{-1} and reduces to near zero at the low-q cutoff.

There are two scattering ranges resulting from the two sample-to-detector distances used, implying two different low-q cutoff values. If, as seen here, the $I \times q$ values are not zero at the low-q cutoff point, there will be a systematic difference between the effective invariants calculated for different q_{min} values. Volume plots for the two scattering ranges employed here indicate a significant systematic difference for the effective invariant calculated from the two regions. For this reason, the effective invariant was not used as a quantitative measure of the craze contribution to the total strain, as has been reported in the literature.[5,15]

Two-dimensional scattering patterns compensated for detector effects are shown in Figure 6. Prior to any deformation, the patterns appear isotropic, with scattering due only to the polymer chains and additives. After craze formation, the pattern consists of two streaks associated with craze wall and craze fibril scattering. These two streaks become readily apparent when background subtraction has been performed. The presence of distinct streaks can be considered to be unambiguous evidence of crazing while the absence of isotropic scattering above background is an indication that cavitation is not present in a significant way.[20] It is worth noting that the two scattering bands are not perfectly perpendicular to each other, making a two-dimensional detector essential for accurate measurements of the craze fibrils. This lack of perpendicularity is not inconsistent with TEM pictures of crazes[19] and, in this instance, could be the result of local anisotropic stresses caused by elongated rubber particles. Such particles have been observed in similar HIPS materials, as reported in an earlier work.[34]

If two distinct deformation processes occurred sequentially, such as rubber-particle cavitation followed by crazing, then distinct stages in the development of the scattering profiles would be anticipated, with changes in the shape of the scattering profile between temporal

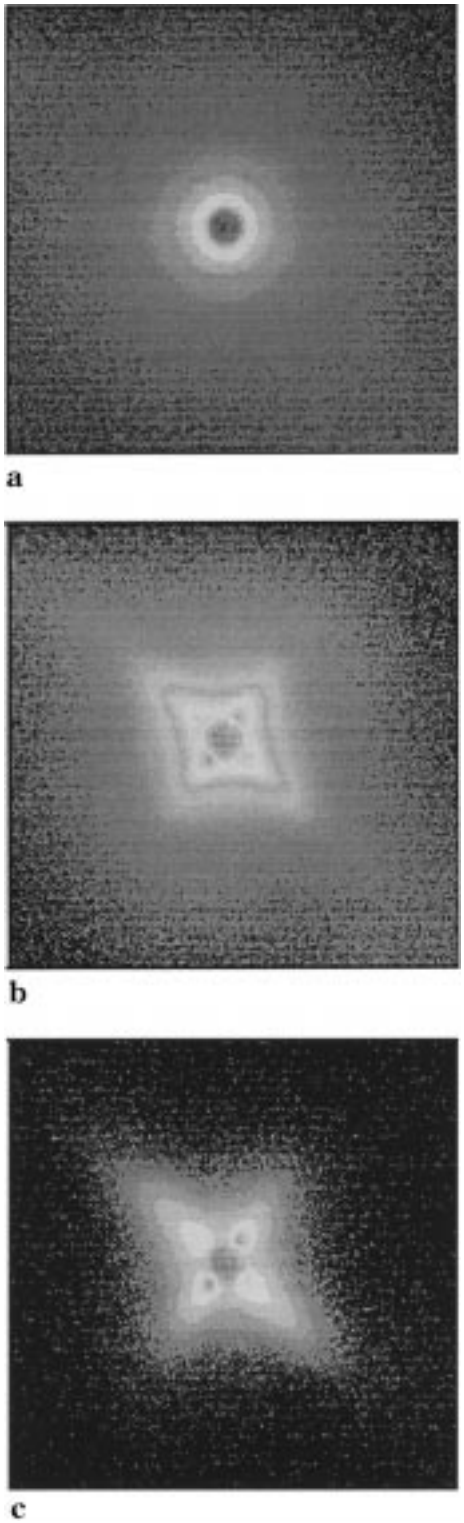

Figure 6. Two-dimensional scattering patterns for HIPS at 70 °C: scattering before applied stress (a); scattering after crazes have formed (b); background subtracted craze scattering (c).

stages. Log−log plots of the reduced one-dimensional data, which illustrate the time-development of the SAXS profiles, are shown in Figure 7. From this figure it can be seen that the entire form of the scattering pattern develops simultaneously, indicating that the entire structure forms coincidentally and must therefore be associated with a single process.

It has been shown in a companion paper[21] that the different regions of the scattering curve can be at-

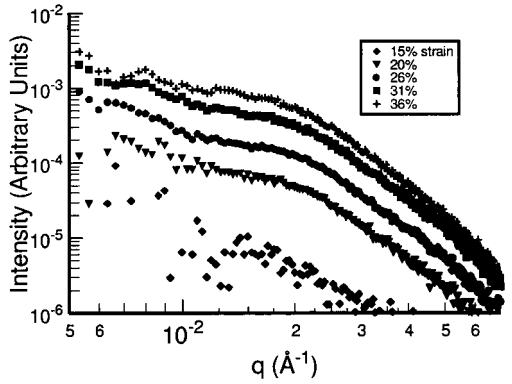

Figure 7. Time-series log−log plot of HIPS at T = 55 °C showing the development of the scattering pattern.

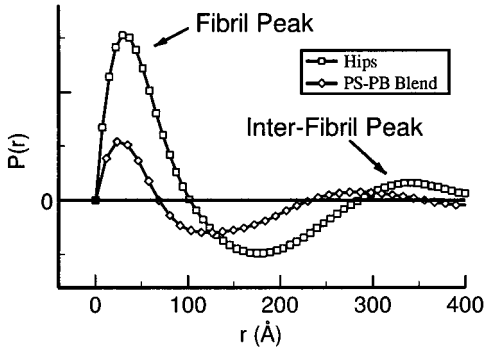

Figure 8. Pair distribution functions obtained from low-*q* range data of HIPS (□) and PS−PB blend (◇) samples at 65 °C.

tributed to the craze fibril structure taken as a whole, with the low-*q* region corresponding to inter-fibril length scales. It can, therefore, be concluded that rubber-particle cavitation is not a precursor to crazing, nor does it accompany the craze process. This supports the observations from Figures 3 and 6 that the deformation process observed by the scattering can only be attributed to the growth of craze fibrils and that no isotropic void formation occurs.

It has been suggested by Magalhaes et al.[15] that the low-*q* scattering observed is due to rubber particle cavitation occurring prior to the formation of crazes. In that work the scattering was divided into separate components due to crazing and void formation. This separation was then used to calculate an invariant which is solely due to crazing. However, real-time studies were not performed, and thus it was not possible to verify that the preferential development of the low-*q* portion of the scattering profiles occurred prior to the development of scattering attributed to crazing, and thus originated from precraze particle cavitation. It is also worth noting that the slopes of the low-*q* regions in the curves reported by Magalhaes et al. are quite different from those observed here, suggesting that the materials follow different deformation processes.

Pair distribution functions obtained for HIPS and PS−PB blend samples are shown in Figure 8. A primary maximum between 25 and 35 Å is observed, with a secondary shallow peak reducing gradually to zero at larger *r* values. The secondary maximum occurs at about 350 Å in the HIPS material, and at about 275 Å in the PS−PB blend. A region of negative *P*(*r*) between the two peaks is present for both materials. In terms of known structures, peaks at small *r* values correspond to the single particle structure of craze fibrils, negative

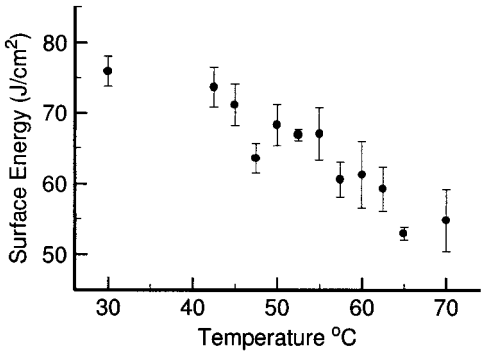

Figure 9. Weighted average of surface energy as a function of temperature for the HIPS material.

regions correspond to voids between fibrils, and shallow positive regions are associated with interfibril scattering. These results are consistent with the interpretation that the scattering observed is due solely to the craze fibril structure.

The two materials give similar *P*(*r*) shapes for the temperatures considered, but the PS−PB blend material has all the above-mentioned features occurring at slightly smaller lengthscales than in HIPS. *P*(*r*) for the PS−PB blend material reaches 0 by 400 Å, while *P*(*r*) from HIPS is still positive at this point. This indicates a higher mobility in the HIPS matrix leading to a greater degree of coherence between fibrils.

3.2. Surface Energy Calculations. The energy to form new craze fibril surface, Γ_f, was determined from the product of applied stress and fibril diameter, as given by

$$\sigma_a = 8\frac{\Gamma_f}{\xi \bar{D}_s} \tag{11}$$

with σ_a being the applied stress, $\bar{D}_s$ being the fibril diameter calculated from the *sigmoidal-gradient* model, and ξ a constant, which can be approximated as unity. This equation is obtained from the *meniscus instability* model by treating the polymer material as a viscous fluid.[19] It does not take into account the extensive diffuse boundaries of craze fibrils which have recently been shown to exist.[21] However, if the fibril density is observed to follow a Gaussian distribution, as assumed here, eq 11 represents a mean surface energy obtained from the approximation of a density-weighted fibril diameter. This approximation will tend to obscure variations in the diffuse boundary width, which should be reflected in the surface energy.

Surface energy calculations were performed for each scattering measurement after the onset of crazing and are observed to be constant for the duration of the crazing in each sample, in keeping with the predictions of the *meniscus instability* model for craze growth. Weighted averages of the energy values for each sample are shown as a function of temperature in Figure 9.

From a microscopic viewpoint, the surface energy is expected to be constant with temperature at low temperatures, where fibril growth proceeds by chain scission, and to decrease with temperature at high temperatures, where fibril growth proceeds by forced reptation. It is not possible from this data to identify a transition point between regions of chain-scission dominated and reptation-dominated craze growth. A more thorough test of the temperature dependence of fibril diameters is required to verify the existence of a measurable transi-

tion between growth mechanisms within the context of current models of fibril surface energy.

4. Conclusions

Two sample materials, HIPS and a solvent-toughened PS−PB blend, have been examined at temperatures between 30 and 70 °C. Both materials were observed to undergo extensive crazing. In the HIPS material, this was preceded by a period of shear deformation, while in the PS−PB blend, crazing was observed to begin at the onset of tensile stress. It was also noted that the craze fibril structure is similar in the two materials with slightly larger length scales in HIPS, pointing to an increased mobility in the matrix. This complements initial observations that the yield point in the PS−PB blend occurs at higher stress values, followed by rapid failure. Surface energy results have been examined in light of the molecular-level predictions of polymer chain dynamics. However, the present results are inconclusive in identifying a scission-to-reptation transition. This transition in deformation mechanism has been observed in pure PS thin films.[2] The presence of rubber additives may result in a broadened transition with considerable overlap of deformation mechanism, which would only be observable with more detailed temperature measurements. The limitations of the surface energy parameter in accounting for diffuse craze fibrils may also be a possible source of these inconclusive observations.

A precise interpretation of the scattering from craze fibrils has been developed which enables the extraction of detailed information of the craze structure. To further this work, the surface energy parameter, derived from the *meniscus instability* model, should be redefined to include finite fibril−void boundaries. A detailed temperature mapping of the tensile stress response, in conjunction with a sufficiently precise definition of the craze fibril surface energy, can then be used to clearly identify the predicted scission-to-reptation transition in chain motion. The ability to obtain information at this level of precision provides a means to perform reliable tests of structure−property relationships as well as a method for examining the validity of current theories of forced reptation.

Acknowledgment. The authors would like to thank S. Gillen of the Department of Physics, Queen's University, for designing and building the motor controller. The authors would also like to thank the technical support staff of the Physics Department, Queen's University, for their assistance in designing and building the apparatus. The authors would like to acknowledge the assistance of Dr. L. A. Utracki of Industrial Materials Institute (IMI) and Dr. Mark Cranch of DOW Canada in providing the samples. This research is supported by the Ontario Center for Materials Research under Contract No. QP2-605 and the natural Sciences and Engineering Council of Canada under Grant No. OGP0045165. The research was carried out (in part) at the National Synchrotron Light Source, Brookhaven National Laboratory, which is supported by the U.S. Department of Energy, Division of Materials Sciences and Division of Chemical Sciences (DOE Contract No. De-AC0276CH00016).

References and Notes

(1) Kausch, H.; Plummer, C. *Polymer* **1994**, *35*, 3848−3857.
(2) Plummer, C.; Donald, A. *Macromolecules* **1990**, *23*, 3929−3937.
(3) Argon, A.; Cohen, R.; Gebizlioglu, O.; Schwier, C. Crazing in Block Copolymers and Blends. In *Advances in Polymer Science*; Kausch, H., Ed.; Springer-Verlag: Berlin, 1983; Vol. 52/53 Crazing in Polymers.
(4) Gebizlioglu, O.; Argon, A.; Cohen, R. *Polymer* **1985**, *26*, 519−528.
(5) Bubeck, R.; Buckley, D., Jr.; Kramer, E.; Brown, H. *J. Mater. Sci.* **1991**, *26*, 6249−6259.
(6) Brown, H.; Argon, A.; Cohen, R.; Gebizlioglu, O.; Kramer, E. *Macromolecules* **1989**, *22*, 1002−1004.
(7) Gebizlioglu, O.; Beckham, H.; Argon, A.; Cohen, R.; Brown, H. *Macromolecules* **1990**, *23*, 3968−3974.
(8) Kinloch, A.; Young, R. *Fracture Behavior of Polymers*; Elsevier Applied Science: New York, 1993.
(9) Bubeck, R.; Blazy, J.; Kramer, E.; Buckley, D.; Brown, H. Real-Time Small-Angle X-ray Scattering Measurements of HIPS and SBS During Tensile Impact. *Mater. Res. Soc. Symp. Proc.*, **1987**, *79*.
(10) Dompas, D.; Groeninckx, G. *Polymer* **1994**, *35*, 4743−4749.
(11) Brown, H.; Kramer, E. *J. Macromol. Sci. Phys.* **1981**, *B19*, 487−522.
(12) Brown, H.; Sindoni, Y.; Kramer, E.; Mills, P. *Polym. Eng. Sci.* **1984**, *24*, 825−832.
(13) Bubeck, R.; Blazy, J.; Kramer, E.; Buckley, D.; Brown, H. *Polym. Commun.* **1986**, *27*, 357−360.
(14) Hristov, A.; Yee, A.; Xie, L.; Gidley, D. *Polymer* **1994**, *35*, 4287−4292.
(15) Magalhães, A.; Borggreve, R. *Macromolecules* **1995**, *28*, 5841−5851.
(16) Salomons, G.; Singh, M.; Gupta, J.; Foran, W.; Clarke, J.; Capel, M. *Rev. Sci. Instrum.* **1996**, *67*, 1748−1752.
(17) Capel, M.; Smith, G.; Yu, B. *Rev. Sci. Instrum.* **1995**, *66*, 2295−2299.
(18) Cullity, B. D. *Elements of X-Ray Diffraction*; Addison-Wesley: Reading, MA, 1959.
(19) Kramer, E. Microscopic and Molecular Fundamentals of Crazing. In *Advances in Polymer Science*; Kausch, H., Ed.; Springer-Verlag: Berlin, 1983; Vol. 52/53 Crazing in Polymer.
(20) Ijichi, Y.; Kojima, T.; Suzuki, Y.; Nishio, T.; Amemiya, Y. *Macromolecules* **1993**, *26*, 829−835.
(21) Salomons, G.; Singh, M.; Bardouille, T.; Foran, W.; Capel, M. *J. Appl. Cryst.*, in press.
(22) Svergun, D. *J. Appl. Crystallogr.* **1992**, *25*, 495−503.
(23) Svergun, D. *J. Appl. Crystallogr.* **1993**, *26*, 258−267.
(24) Glatter, O. *J. Appl. Crystallogr.* **1977**, *10*, 415−421.
(25) Glatter, O.; Kratky, O. *Small Angle X-ray Scattering*; Academic Press: London, 1992.
(26) Feigin, L.; Svergun, D. *Structural Analysis by Small-Angle X-ray and Neutron Scattering*; Plenum Press: New York, 1987.
(27) Lin, T.; Tsao, C. *J. Appl. Crystallogr.* **1996**, *29*, 170−177.
(28) Svergun, D.; Semenyuk, A. *Manual of Program Package GNOM*; E4.2 ed.; 1993 (unpublished; private communication).
(29) Ruland, W. *J. Appl. Crystallogr.* **1971**, *4*, 70−73.
(30) Koberstein, J.; Morra, B.; Stein, R. *J. Appl. Crystallogr.* **1980**, *13*, 34−45.
(31) Lazzeri, A.; Bucknall, C. *J. Mater. Sci.* **1993**, *28*, 6799−6808.
(32) McCrum, N.; Buckley, C.; Bucknall, C. *Principles of polymer engineering*; Oxford University Press: New York, 1988.
(33) Kramer, E.; Berger, L. Craze Growth and Fracture. In *Advances in Polymer Science*; Kausch, H., Ed.; Springer-Verlag: Berlin, 1990; Vol. 91/92 Crazing in Polymers.
(34) Salomons, G.; Singh, M.; Hiltz, L.; Pan, L.; Newson, W. *Nucl. Instrum. Methods B* **1995**, *97*, 282−286.

MA980709E